Safe nanoengineering and incorporation of transplant populations in a neurosurgical grade biomaterial, DuraGen Plus™, for protected cell therapy applications

Louise Finch[1], Sarah Harris[6], Georgios Solomou[1], Jon Sen[1], Nikolaos Tzerakis[2], Richard D Emes[3,4], Catherine S Lane[5], Sarah R Hart[1], Christopher F Adams[6] and Divya M Chari [1,*]

[1]School of Medicine, Keele University, Stoke-on-Trent, ST5 5BG; d.chari@keele.ac.uk, Louise.Finch5@nhs.net, j.sen@keele.ac.uk, s.r.hart@keele.ac.uk

[2]Neurosurgery department, University Hospitals of North Midlands, Stoke-on-Trent, ST4 6QG; Nikolaos.Tzerakis@uhnm.nhs.uk.

[3]Advanced Data Analysis Centre, University of Nottingham, Sutton Bonnington, Leicestershire, LE12 5RD, UK.

[4]School of Veterinary Medicine and Science, University of Nottingham, Sutton Bonnington, Leicestershire, LE12 5RD, UK; Richard.Emes@nottingham.ac.uk.

[5]Sciex, Phoenix House, Lakeside Drive, Centre Park, Warrington WA1 1RX; Cathy.Lane@sciex.com.

[6]Faculty of Natural Sciences, Keele University, Stoke-on-Trent, ST5 5BG; c.adams@keele.ac.uk, s.j.harris@keele.ac.uk

*Correspondence: d.chari@keele.ac.uk

Abstract

High transplant cell loss is a major barrier to translation of stem cell therapy for pathologies of the brain and spinal cord. Encapsulated delivery of stem cells in biomaterials for cell therapy is gaining popularity but experimental research has overwhelmingly used laboratory grade materials unsuitable for human clinical use - representing a further barrier to clinical translation. A potential solution is to use neurosurgical grade materials routinely used in clinical protocols which have an established human safety profile. Here, we tested the ability of Duragen Plus™ - a clinical biomaterial used widely in neurosurgical duraplasty procedures, to support the growth and differentiation of neural stem cells- a major transplant population being tested in clinical trials for neurological pathology. Genetic engineering of stem cells yields augmented therapeutic cells, so we further tested the ability of the Duragen Plus™ matrix to support stem cells engineered using magnetofection technology and minicircle DNA vectors- a promising cell engineering approach we previously reported (Journal of Controlled Release, 2016 a &b). The safety of the nano-engineering approach was analysed for the first time using sophisticated data-independent analysis by mass spectrometry-based proteomics. We prove that the Duragen Plus™ matrix is a promising biomaterial for delivery of stem cell transplant populations, with no adverse effects on key regenerative parameters. This advanced cellular construct based on a combinatorial nano-engineering and biomaterial encapsulation approach, could therefore offer key advantages for clinical translation.

Keywords: neural stem cell; biomaterial; combinatorial therapy; genetic engineering; magnetofection; DNA minicircles; mass spectrometry, SWATH, proteomics

1. Introduction

Injury in the central nervous system (CNS) is associated with a complex, multifaceted pathology [1,2] and it is widely believed that combinatorial therapies targeting multiple therapeutic targets are needed to promote effective repair. Numerous preclinical studies have demonstrated improved functional and histological outcomes following transplantation of genetically engineered neural stem cells (NSCs). Potential mechanisms include replacement of cells lost to the injury processes, release of pro-regenerative factors and additional expression of therapeutic proteins, for example, neurotrophic factors to encourage nerve fibre growth or enzymes to break down glial scar constituents [3–8]. Phase I/II trials investigating NSC transplantation for stroke and amyotrophic lateral sclerosis are ongoing [9] demonstrating the potential to translate these approaches into the clinic. Despite this promise, a major barrier to translation of neural cell therapy is the high cell loss that occurs post-transplantation into the CNS, due to factors such as high mechanical forces and cell clumping during delivery through fine gauge needles and cell washout from lesion sites. In general, < *ca* 3% of cells will be engrafted post-transplantation [10,11] with one study showing that no transplanted fetal neuroepithelial stem cells survived at three days post-transplantation [12]. These issues pose major clinical challenges as high cell death reduces the efficacy of the therapy, could induce secondary inflammatory responses and increase expense due to higher cell numbers needed for initial transplantation procedures.

Such factors have led to a major drive to develop biomaterial based delivery technology deploying implantable and protective scaffolds for stem cell delivery. Functional neurological improvement has been shown after encapsulated NSC delivery into various rodent models of CNS injury/disease. Poly lactic-co-glycolic acid (PLGA) scaffolds protected NSC transplants in a rat lateral hemisection injury model leading to improved locomotion whereas NSCs transplanted alone led to scarring, cyst formation and poorer behavioural outcomes [13]. Using a fibrin matrix, human NSCs were successfully implanted into complete transecting injuries in rats leading to axon extension from the graft and from the host tissue with improved behavioural scores compared to no graft implantation [14]. Gelfoam scaffolds [15], porous collagen scaffolds [16] and 3D gelatin-electrospun poly (lactide-co-glycolide)/PEG scaffolds [17] all improved functional recovery when used to deliver NSCs into rat models of SCI. *Critically, however, such biomaterials are not yet clinically approved and lack the scalable manufacturing processes needed for adoption into clinical practice.* This is a major issue as the FDA estimate that on average new biomaterial scaffolds take seven years to proceed through FDA-approval [18].

Neurosurgical grade biomaterials which have been approved for human use could offer a suitable potential alternative. In particular, Duragen Plus™ matrix is a medically approved, neurosurgical grade biomaterial derived from Type I bovine collagen, and predominantly used in duraplasty procedures. Here, it allows for the infiltration of fibroblasts for restoration and repair of the dura mater following a breach made intraoperatively and is reported to be resorbed after six to eight weeks [19]. The material is reported to lack immunogenicity, cytotoxicity and pyrogenicity and is conformable, sterile and biocompatible [20]. Duragen Plus™ has been implanted into the nervous system with no adverse effects noted and supports neural cell growth, including that of rat cortical neurons [21]. Despite these critical advantages, the application of Duragen Plus™ to support encapsulation of stem cells for NSC therapy has never been evaluated.

We have tested the utility of the Duragen Plus™ matrix to support incorporation and growth of unmodified NSCs, and those genetically nanoengineered with magnetic nanoparticles and minicircle DNA vectors. Our aims are to (i) examine whether NSCs can be propagated in the neurosurgical grade biomaterial scaffold; (ii) confirm the safety of nanoengineering NSCs with subsequent incorporation into Duragen Plus™ using histological assays and mass spectrometry coupled with bioinformatics.

2. Results

2.1. Structural Characterisation of Duragen Plus™

Duragen Plus™ demonstrated the ability to rapidly absorb tissue culture medium (within 5-10 seconds) (**Figures 1a-b**) indicating a highly porous matrix structure. From a gross visual assessment, ca. 25-40% volumetric expansion of the material was observed as the medium was absorbed. Under light microscopy, Duragen Plus™ demonstrated an obvious, highly porous structure (**Figure 1c**). In preliminary experiments, clusters of NSC nuclei could be easily detected within the material pores after seeding cells directly onto the matrix (**Figure 1d**). Scanning electron microscopy (SEM) of Duragen Plus™ confirmed its highly porous structural network (**Figures 1e-f**) with variable pore sizes whose average size was 25.93 ± 14.31 μm (range 5.12 – 90.41 μm).

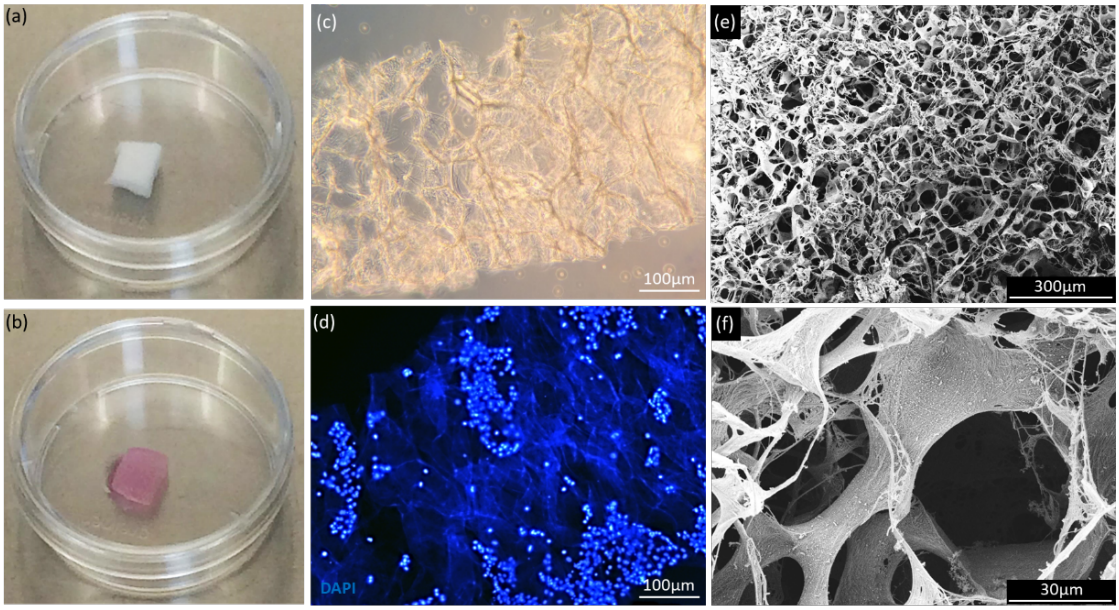

Figure 1: Porous Duragen Plus™ structure demonstrates cell infiltration and attachment. *(a) Dry Duragen Plus™ sample before processing. (b) Duragen Plus™ after application of cell medium demonstrates fluid absorption with evidence of swelling. (c) Duragen Plus™ under light microscopy demonstrates an obvious porous structure. (d) Clusters of NSC nuclei could be observed which appear to infiltrate these pores and adhere to the Duragen Plus™ matrix fibres. (e) and (f) SEM at x100 magnification and x1000 magnification respectively show the highly porous structure of Duragen Plus™.*

2.2 NSCs showed high viability and normal "stemness", proliferative capacity and differentiation in Duragen Plus™

To assess the safety of the biomaterial for NSC growth, assays of live and dead cells along with counts of pyknotic nuclei were carried out at early (24 h), intermediate (eight days) and late (12 days) time points. Pyknosis (defined as the condensation of chromatin within the nucleus caused by necrosis or apoptosis) was detected by evidence of a hyperdense, small and/or fragmenting nucleus [22]. NSCs and differentiated cells displayed high cell viability across all time points (≥87.0 ± 3.74%) and a low proportion of pyknotic nuclei (≤7.48 ± 1.51%) (**Figures 2a, c-d**). There was no significant difference between the proportions of live cells or pyknotic nuclei in Duragen Plus™ at any time point examined.

In Duragen Plus™, a high proportion of nuclei were positive for nestin, an NSC cytoskeleton marker (93.87 ± 2.84%) and Sox-2, an NSC-specific transcription factor (95.53 ± 0.42%) at 48 h. Cells demonstrated typical NSC morphologies with bipolar processes and were associated with round, healthy appearing nuclei (**Figure 2e-f**). SEM confirmed the presence

of clusters of neurospheres, clearly incorporated within the Duragen Plus™ matrix (**Figure 2b**). At all time points investigated, there was clear evidence of cell proliferation (**Figures 2f&h and Figures 2g&h)**). At 24 h, 25.59 ± 4.07% of cells expressed the proliferation marker, EdU (**Figure 2f**). This significantly decreased to 7.21 ± 1.41% at eight days once the cells had differentiated. The majority of cells (ca. 70%) that showed EdU labelling in the differentiated population were identified as GFAP positive astrocytes (**Figure 2g**). NSCs and their differentiated progeny appeared to be evenly distributed throughout the 3D depth of the matrix with similar numbers of cells counted at each plane of analysis (PoA) and no statistical differences detected between these (**Figures 2i-j**).

Six days after induction of differentiation (eight days growth in Duragen Plus™), the three major classes of daughter cells of NSCs, viz. neurons, astrocytes and oligodendrocytes were all observed within the biomaterial matrix. The highest proportion (79.58 ± 6.28%) of cells was that of astrocytes which demonstrated characteristic stellate morphologies (**Figure 3a**). 18.61 ± 5.10% of cells were of the neuronal lineage, staining for the neuronal marker Tuj1 (**Figure 3a**). The smallest proportion of cells were oligodendrocytes, staining positive for MBP (2.12 ± 0.96%) which displayed highly branched morphologies often extending into multiple planes within the biomaterial matrix (**Figure 3a**). The relative proportions of each cell type generated were similar across all examined time points (**Figure 3b**). Neurons demonstrated evidence of cellular maturation across the time period examined displaying increasing complexity in their networks (**Figure 3a**) and a statistically significant increase in axon length from day eight to day 16 (**Figure 3c**).

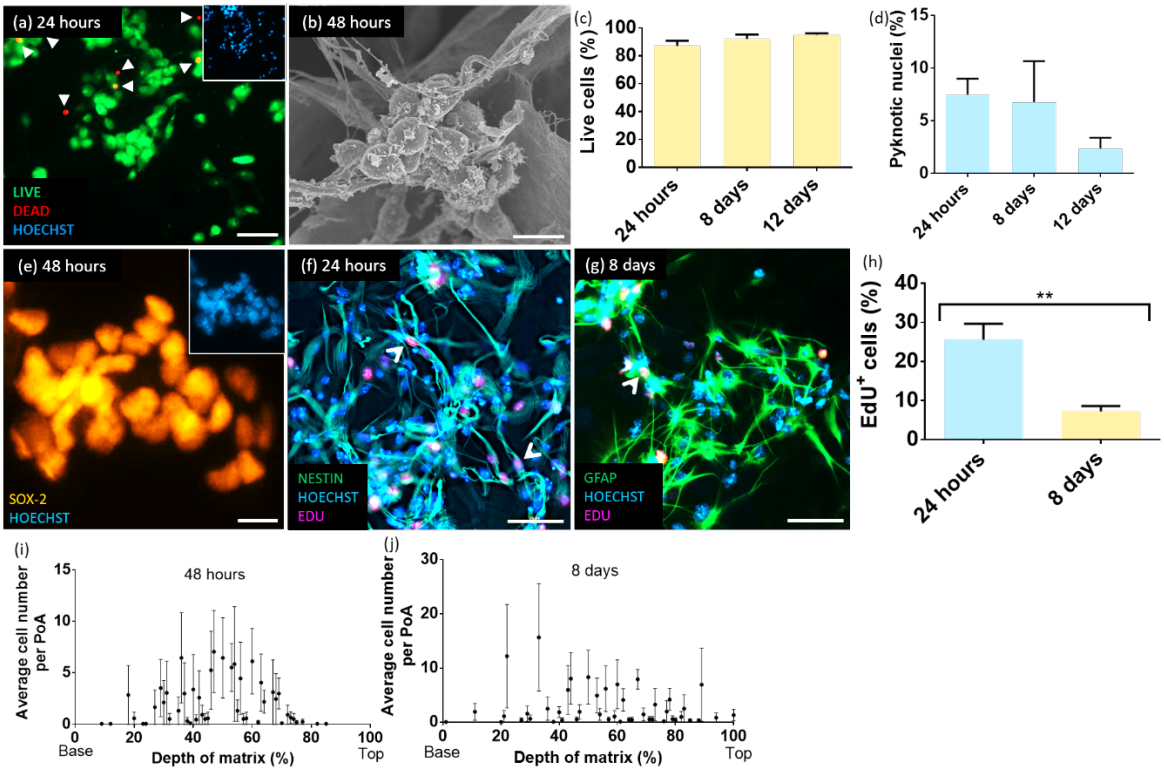

Figure 2: Duragen Plus™ supports NSC survival, maintenance of stem cell phenotype and proliferation in a 3-D matrix. *(a) Representative fluorescence image at 24 h demonstrating live cells stained with calcein and dead cells stained with ethidium homodimer-1 (arrows indicate dead cells). The insert is a counterpart image showing the nuclei stained with Hoechst dye. Scale bar = 50 µm. (b) SEM image of NSCs growing in Duragen Plus™ matrix at 48 h. Scale bar = 15 µm. (c) Bar graph displaying cell viability within Duragen Plus™ across all time points. The difference between time points was not significant (p-value = 0.179, one-way ANOVA, n=3). (d) Bar graph displaying proportions of pyknotic nuclei detected in NSCs grown within Duragen Plus™ across all time points. The differences between time points were not significant (p-value = 0.297, one-way ANOVA, n=3). (e) Representative fluorescence image of Sox-2 staining of NSCs in Duragen Plus™. 95.5 ± 0.42% of cells were positive for Sox-2 at 48 h (n=3). Scale bar = 10 µm. (f) Representative fluorescence images demonstrating proliferation of NSCs (nestin positive cells) observed at 24 h in Duragen Plus™, arrows indicate proliferating NSCs, scale bars = 50 µm and (g) proliferation of differentiated cells. Arrow indicates a proliferating astrocyte in the biomaterial matrix (GFAP positive cell). (h) Bar chart showing numbers of proliferating cells detected within Duragen Plus™ at 24 h and 8 days (**p-value < 0.01, two sample T test, n=3). Graphs (i-j) demonstrate 3-D distribution of cells throughout the Duragen Plus™ construct at 48 h and eight days.*

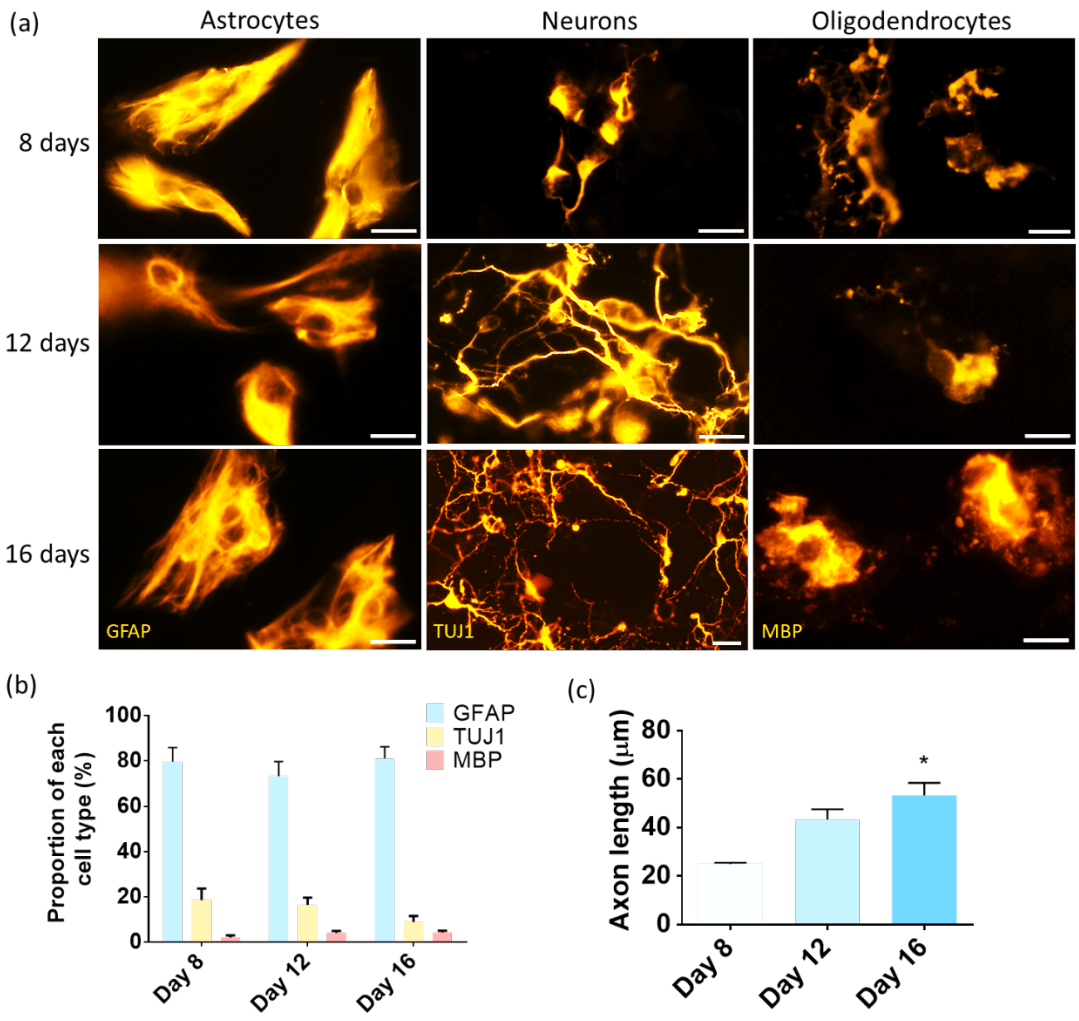

Figure 3: ***Duragen Plus™ supports NSC differentiation and maturation of daughter astrocytes, neurons and oligodendrocytes.*** *(a) Representative fluorescence image panel demonstrating maturation of astrocytes, neurons and oligodendrocytes at day eight, 12 and 16 in Duragen Plus™. Scale bar = 25 μm. Bar graph (b) demonstrates the differentiation profile of NSCs in Duragen Plus™. (c) Axon length increased two-fold from day eight to day 16. Statistical difference is: *p-value < 0.05 (one-way ANOVA with Bonferroni multiple comparison tests, n=3).*

2.3 Duragen Plus™ supports growth of genetically nano-engineered NSCs: cell engineering protocols show minimal impact on NSC molecular profiles

Neurospheres were magnetofected with GFP encoding minicircles using our previously developed procedures [23,24]. At 24 h post-transfection, the engineered NSC population was split into parallel experiments for proteomic analysis or for incorporation into Duragen Plus™ by direct seeding into the matrix. At 24 h after seeding (48 h after transfection), GFP

production was observed in NSCs within the Duragen Plus™ matrix (**Figure 4a-d**), indicating transfection processes continued as expected within the biomaterial matrix. Due to the high density of NSCs within neurospheres, individual NSCs expressing GFP could not be identified for quantification purposes. However, it was observed that a high proportion of neurospheres within Duragen Plus™ demonstrated at least one NSC showing GFP production, detected by an anti-GFP antibody (82.03 ± 3.55%).

The other subset of engineered NSCs were lysed at two and four days after magnetofection for proteome analysis using SWATH-MS data independent acquisition (DIA). Comparison between treated and untreated control cells made using Principal Components Analysis (OneOmics platform) (**Figure 4e**) demonstrates similarity of the samples. The litter from which the cells were harvested was the greatest differentiator between samples, followed by the number of days post-harvest. High technical reproducibility of each triplicate injection was observed, with close clustering of technical replicates (**Figure 4e**). Detailed investigation of the proteins identified by SWATH-MS further indicated that few system-wide changes were observed following magnetofection with minicircle vectors (**Figure 4f-g**). These changes were fewer in number than those delineating cells at day four of the experiment vs. day two (**Figure 4h)**. The full list of putatively differentially-expressed proteins is provided as supplementary tables 1-4. Whilst most of the proteins identified have no known association with NSC viability, proliferation or differentiation (factors that we consider key for effective transplantation), a downregulation of GFAP (-2.4-fold, p=0.002) was observed in transfected NSCs compared to control NSCs at day four. This was less pronounced than the alteration observed for control cells over the time period day two to day four (15.6-fold-change, p=3E-6).

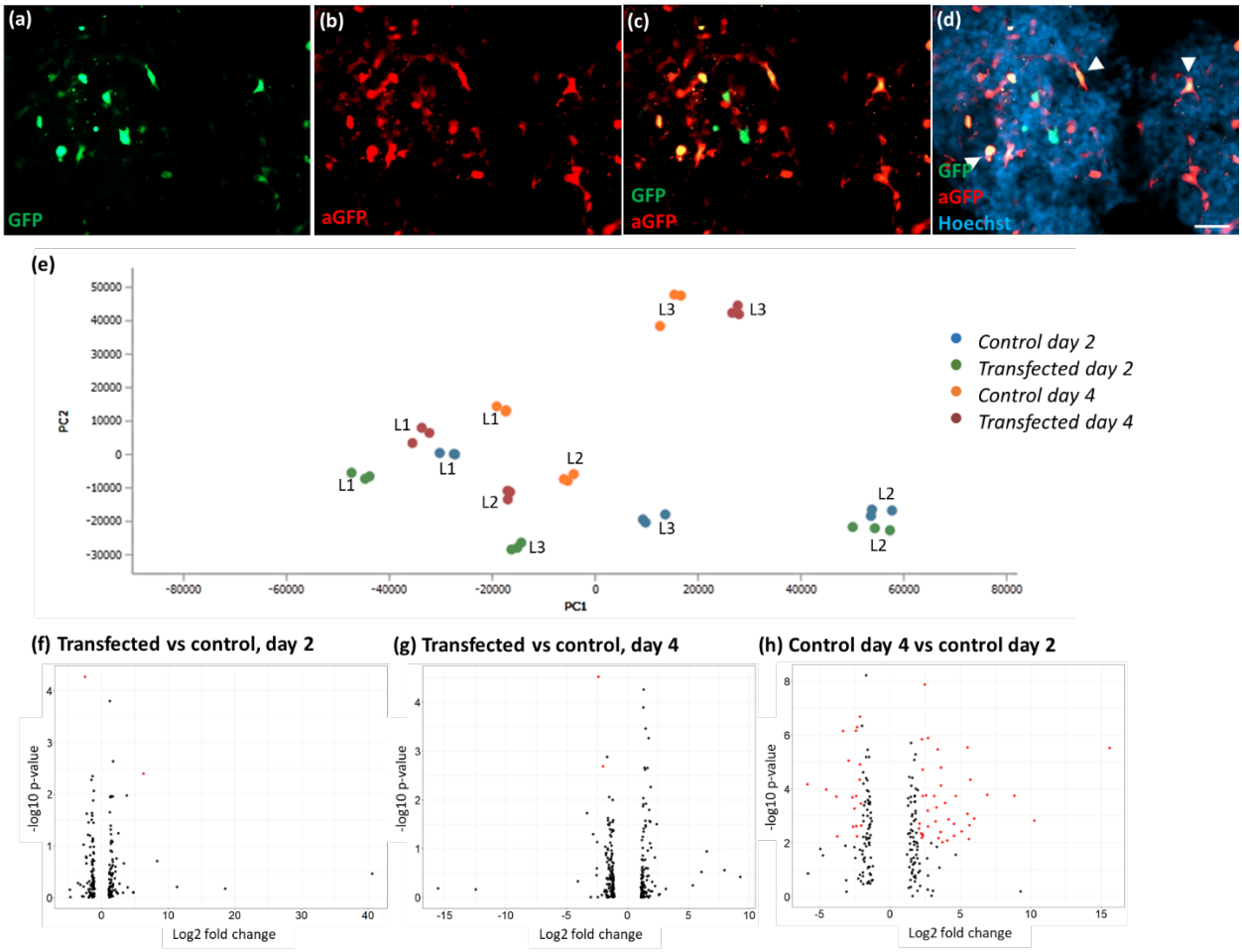

Figure 4: Proteomic analysis of NSCs reveals minicircle/nanoparticle safety for engineering of pre-incorporated cells. *(a-d) Representative counterpart fluorescence images of minicircle magnetofected NSCs in Duragen Plus™, 48 h after transfection: (a) GFP production (b) anti-GFP antibody (aGFP) detecting GFP production, (c) double merged image displaying GFP expression detectability increased by the anti-GFP antibody and (d) triple merged image demonstrating the proportion of NSCs producing GFP within the Duragen Plus™ matrix. Arrowheads indicate NSCs producing GFP (green) and stained positive for anti-GFP (red). Scale bar = 50 µm. (e) Principal Components PC1/PC2 plot of global patterns of protein expression. Clusters labelled L1-L3 show results obtained from individual litters. Blue = Control Day 2; green = minicircle-MNP-treated, Day 2; orange = control day 4; red = minicircle-MNP-treated day 4. (f-h) Volcano plots plotted as log_2 most likely ratio fold-change vs. $–log_{10}$ p value. Significantly dysregulated proteins ($p<0.01$, ≥2-fold change at 65% confidence, 0.2 reproducibility, excluding single peptides) are shown in red. Changes between untreated and treated NSCs at (f) day 2 and (g) day 4; (h) observed changes between control NSCs at day 2 and day 4.*

2.4 Histological analysis of genetically engineered NSCs propagated in Duragen Plus™ demonstrates protocol safety and retention of transgene expression

After 24 h growth in Duragen Plus™, the transfected NSC population demonstrated high viability (92.83 ± 2.09%) equivalent to that of the control (95.67 ± 2.18%) (**Figure 5a&c**). Further, there was no statistical difference in the proliferation rates of the transfected NSC population versus the control population (**Figure 5b&d**). At this time point, the majority of cells were positive for nestin and sox-2, with no differences in the proportions of cells labelled with these markers between transfected and control conditions (**Figure 5e-h**). >95% of GFP producing cells at 48 h post transfection were NSCs as evidenced by GFP co-localisation with NSC marker expression. NSC morphologies were also similar across transfected and control groups (**Figure 5e&f**). After differentiation (ten days post transfection, eight days post seeding into Duragen Plus™), all three differentiated cell types were present in the matrix with no differences in the proportions of each cell type when the transfected population were compared to the control population (**Figure 6a-d**). GFP production in Duragen Plus™ was noted up to day ten post transfection in astrocytes, the latest time point examined (**Figure 6a**).

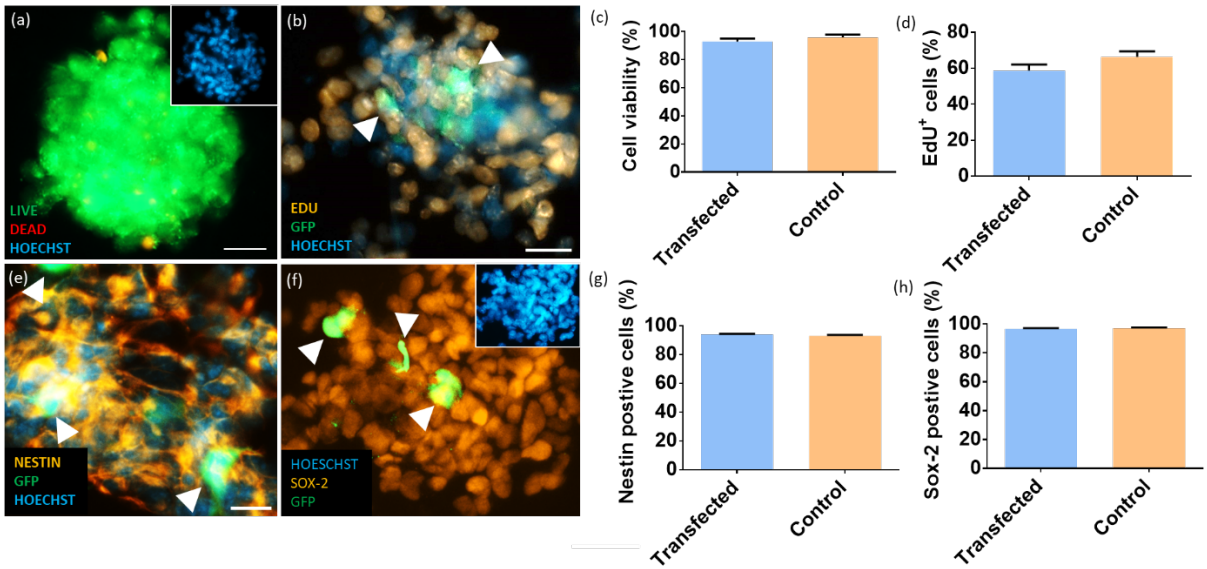

Figure 5: NSC viability, proliferation and stemness unaffected following nanoengineering and incorporation into Duragen Plus™. *(a) Representative fluorescence image of live/dead stained, transfected NSCs in Duragen Plus™ at 48 h post transfection/ 24 h post-seeding in to Duragen Plus™ displaying high viability with no difference to controls (p-value = 0.392, two sample T-test, n=4). (b) Representative fluorescence image of transfected NSCs (arrows) in Duragen Plus™ at 48 h post*

transfection/ 24 h post-seeding in to Duragen Plus™. (e-f) Transfected NSCs within Duragen Plus™ demonstrating a high proportion of nestin positive cells (e) and sox-2 positive cells (f). Arrows indicate GFP producing NSCs. (a-f) Scale bars = 25 µm. Bar graphs (c-h) demonstrate proportions of (c) viable cells at day 2, (d) cells proliferating at day 2, (g) cells expressing nestin at day 2, and (h) cells expressing sox-2 at day 2. No significant differences (p>0.05) between transfected and control NSC populations in Duragen Plus™ were noted (n=4).

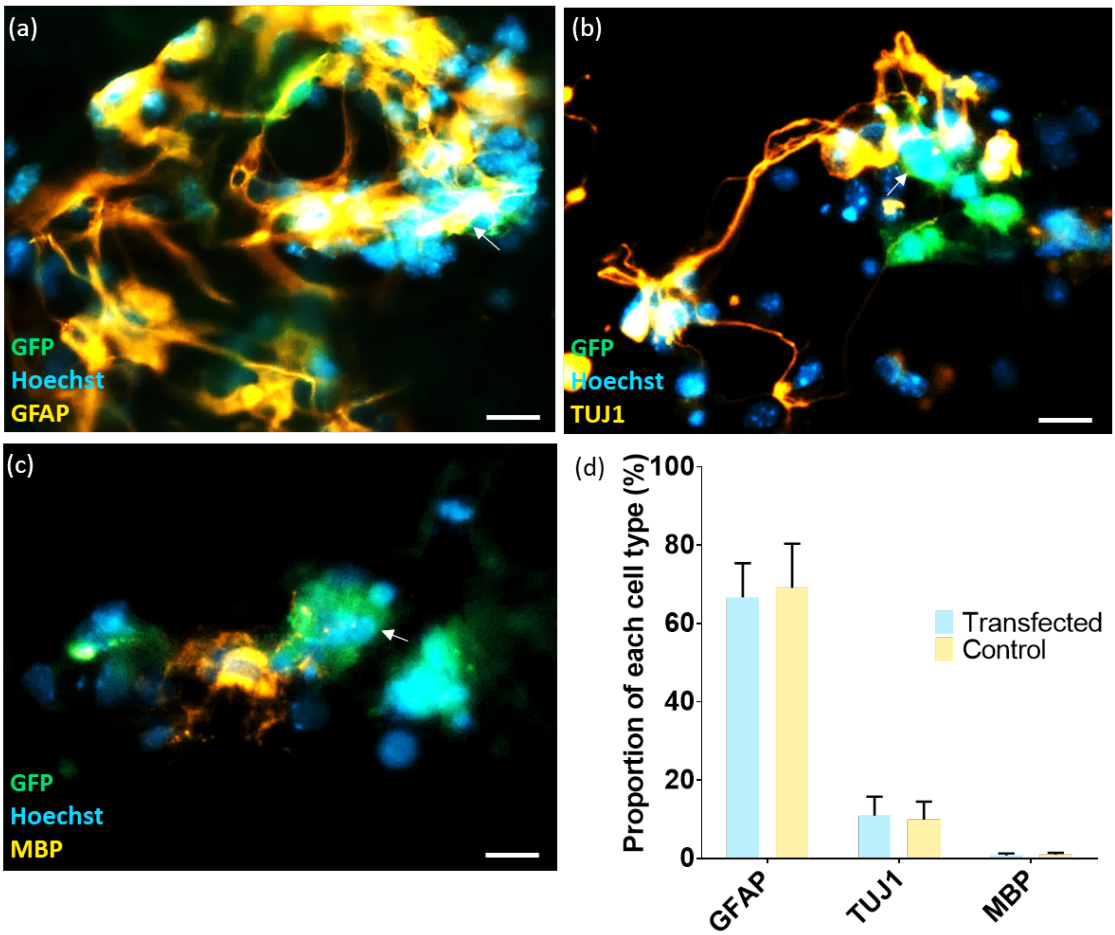

Figure 6: NSCs retain the ability to differentiate into their daughter cells with continued transgene expression within Duragen Plus™. *Representative fluorescence images (a-c) of differentiated transfected NSCs: astrocytes (a), neurons (b) and oligodendrocytes (c) display normal morphologies within the construct at ten days post transfection/ nine days post-seeding in to Duragen Plus™. Arrows indicate GFP producing cells with the morphological appearance of astrocytes. (a-c) Scale bar = 25 µm. Bar graph (d) demonstrates relative proportions of each cell type in transfected and control populations. Proportions of each cell type do not differ between control and transfected cells (p-values > 0.05, two sample t-tests, n=4).*

3. Discussion

This is the first demonstration of the capacity of a neurosurgical grade biomaterial to support the growth of NSCs- a major neural transplant population for clinical applications. Our data support the concept that this clinical biomaterial could be used as a cell delivery matrix in neural cell therapy. Laboratory grade biomaterials have been shown to successfully support stem cell growth *in vitro*, with NSCs demonstrating cell survival, normal phenotypic expression and importantly differentiation into neurons in fibrin hydrogels [25], 3D gelatin-electrospun poly (lactide-co-glycolide)/ polyethylene glycol (PEG) scaffolds [17] and poly (L-lactic acid) nanofibers [26]. Functional neurological improvement was reported with NSCs *in vivo* when cultured in a fibrin matrix [14,27], poly lactic-co-glycolic acid (PLGA) scaffold [13,28], gelfoam scaffold [15], porous collagen scaffold [16] and 3D gelatin-electrospun poly (lactide-co-glycolide)/PEG scaffolds [17]. However, these biomaterials are not tested for human use, therefore rigorous trials would be essential prerequisites before clinical translation can be envisaged.

Duragen Plus™ by contrast offers the major benefit that it is pre-approved by the FDA for surgical use. The biomaterial is designed to be pliable for surgical use, allowing it to be moulded to lesions varying in size and shape. The material is porous, facilitating repair processes such as cellular infiltration and vascularisation [29] and to date has no recorded immune rejection events, indicating a strong safety profile. To facilitate regrowth, a scaffold needs to degrade, ideally over a two-to four-month window [30]. Duragen Plus™ when utilised as a dural substitute degrades over a period of two months highlighting its suitability for neurological applications [29]. We have shown that NSCs grown within Duragen Plus™ display high survival, maintenance of stem cell phenotype, continued proliferation and differentiation into all three daughter cell types (without alteration of cell fate), demonstrating the safety of the material. The counts of differentiated NSCs are in the expected proportions as previously observed on standard culture substrates [23,24].

Further, genetically engineered NSCs have been incorporated into the matrix, facilitating potential combinatorial therapy for cell replacement and functional protein delivery into injury sites- highlighting the advantages offered by this material. We have previously discussed that the pathological microenvironment of neural injury sites limits tissue regeneration. Manipulation of injury foci to a pro-regenerative profile, through over-expression of regeneration enhancing molecules can facilitate repair processes such as axonal growth, myelination and cellular organisation with improved survival of transplant populations [24, 31–40, 60] whilst limiting undesirable systemic effects. Pre-clinical and early clinical data support the concept that such an approach offers significant benefits for functional

neurological recovery. Additionally, we have previously highlighted the significant benefits offered specifically by NSCs in such gene delivery approaches, given their role in neural cell replacement in transplantation therapies, release of therapeutic and immunosuppressive factors, and their migratory capacity (including toward sites of pathology) along with their demonstrated therapeutic potential in clinical trials [24, 60].

In terms of cell engineering, we have used a fusion of iron oxide nanoparticle based gene delivery with novel minicircle DNA vectors to genetically engineer the stem cells used here. Translation of genetically engineered cells into the clinic has traditionally been hampered by heavy reliance on viral mediated transfection which is associated with cytotoxicity, altered cell physiology and difficulty with scale up procedures [41–48]. The use of non-viral methods of transfection are thought to have higher translational relevance than viral vectors (given safety concerns with the latter), although are often associated with low transfection efficiencies. By contrast, MNP mediated gene delivery can be enhanced through application of oscillating magnetic fields to efficiencies near those of viruses (e.g. to a maximal efficiency of ca 55%, with transfection persisting up to 30 days, the last time point observed [24]). Minicircles also offer key advantages for biomedical gene engineering over other bacterial plasmids due to their smaller size, lack of antibiotic resistance genes and other potentially inflammatory sequences [24]. They have a higher transfection efficiency and reduced rates of transgene silencing, enabling longer term expression in engineered cells compared to conventional plasmids [24]. Minicircles are also easy to produce and both minicircles and MNP production can be scaled up for clinical applications. For therapeutic gene delivery, we have previously shown that NSCs can be nanoengineered to deliver a gene encoding a major neurotherapeutic factor brain derived neurotrophic factor/BDNF using our technology [49], with improved regenerative outcomes, highlighting the benefits of our approach for genetic modification of the stem cells used.

To date, safety assessments of novel cell engineering technologies have often been relatively crude relying almost exclusively on analyses of cell number, viability and adherence and/or biochemical analysis such as the MTS assay. Indeed, the safety of nanoengineering protocols for NSCs using minicircle DNA vectors and nanoparticles has only been assessed using histological measures to date. Whilst such outcome measures are undoubtedly useful as first-stage readouts of the safety of nanoengineered cells, these cannot provide insights into subtle alterations in cellular physiology or the functional (regenerative) capacity of the cells. As such, it is essential for neuro-nanotechnology studies to develop safety screening systems/protocols for engineered transplant populations with enhanced orders of biological sophistication to evaluate their clinical translational potential. For our genetic engineering experiments using NSCs, we therefore considered it essential to

separate potential adverse effects associated with the cell engineering protocols from those related to biomaterial incorporation. To this end, we utilised a sophisticated proteomics based approach to gain a detailed insight into the physiological ‘normalcy’ of the engineered stem cells pre-incorporation.

Using our advanced approach, we show that the magnetofection process had no discernible effect on key regenerative properties of the NSCs. To the best of our knowledge, this is the first proteomic investigation into the effects of magnetofection on the major transplant population of NSCs or indeed any cell type. A short (48 h) time point was used for the proteomics analyses as this coincides with the timing of peak GFP expression [41,42]; as such, it is reasonable to expect significant cellular and molecular changes at this time if the procedures were negatively impacting safety. In addition, a longer time point (96 h) was also used to examine molecular changes over time and which is in line with the time neurospheres have been cultured prior to transplantation (4-6 days [43,44]; 96 h post-transfection is 5 days in culture). The use of mass spectrometry and bioinformatics based methods to examine potential perturbations to complex cellular behaviours, provides a highly detailed readout of the effect of MNPs, magnetofection protocols and MNP-delivered transgenes for transplantation therapy research. Further, the wide-scale analysis used here provides an unbiased approach unhindered by prior expectation, in contrast to antibody-driven approaches, which by their very nature are target-driven. In addition, protein identification in Western blotting and ELISA requires specific antibodies which are not always available or are poorly characterised [47]. In this regard, mass spectrometry can measure and compare intensities of several different peptides per protein in contrast to the one band available for analysis in Western blotting. Mass spectrometry also combines a high linear dynamic range (up to 5 orders of magnitude linear dynamic range) with high sensitivity (femto- to attomole detection on-column) and mass resolving power (20,000 FWHM), meaning that broad, unbiased analyses can be performed with a high degree of quantitative certainty [48,50]. Use of retention time standards to enable normalisation of peak retention times improves alignment of large datasets and enhances our ability to make direct inferences between SWATH window information and peptide/protein identity and quantity. Therefore, we propose that the molecular approach described here can inform safe and effective neuro-nanomaterial design and MNP application strategies (e.g. use of magnetic fields) allowing for the systematic correlation of biomaterials' properties with safety outcome measures in stem cell transplant populations.

Mass spectrometry results revealed limited changes in proteome profile following nanoengineering, where the vast majority of observed changes were attributable to biological differences between parallel experiments performed using different litters and time

points, with very few major alterations in protein expression being observed as a result of magnetofection. This unbiased proteome analysis revealed the reproducible observation in excess of 20,000 peptides from over 4000 proteins of a wide variety of gene ontologies, providing a wide and deep examination of proteome metrics. GFAP expression was shown to increase over time in both control and transfected cells from day 2 to 4. This may be expected as neurospheres are known to be composed of a heterogeneous cell population containing NSCs and some differentiating cells [51], so this increase could indicate ongoing differentiation in the neurospheres. However, we observed that the increase in GFAP expression over time in transfected samples was not as great as in control samples (2.4 fold less). As we did not see a difference in GFAP expression at day 2, the observed downregulation of GFAP in transfected samples compared to controls could be suggestive of a longer term effect of the nanoparticles on NSC differentiation. Another study has shown a reduction in GFAP expression in response to treatment with cerium oxide nanoparticles but this was performed after 10 days of NSC (C17.2 cells) differentiation [52]. The brain isoform of glycogen phosphorylase (PYGB) was also found to be downregulated in transfected cells at day 4. Glycogen storage and metabolism have been shown to be important for cell cycle maintenance and one study has shown this pathway is involved in regulating astrocyte proliferation [53]. This may also be suggestive of an effect on the astrocyte population within neurospheres – although we do not detect such an effect in our histological analyses. Mitochondrial pyruvate carrier 2 (MPC2) was found to be downregulated in transfected cells compared to control cells at day 2. MPC2 has a role in pyruvate metabolism and there is some evidence showing that pyruvate metabolism can influence stem cell differentiation [54]. However, other proteins within this pathway were not found to be dysregulated and this was not a sustained effect (no dysregulation was found by day 4). Finally, A0A171EBL2 or E3 ubiquitin-protein ligase RNF213 was found to be upregulated in transfected cells at day 2. RNF213 has roles in ligase activity and ATPase activity and has been associated with vascular development and diseases such as Moyamoya disease [55]. No clear involvement in stem cell behaviour could be found for this protein.

Overall, the proteomics data indicates that safe genetic engineering of NSCs can be accomplished using magnetofection and minicircle technology. In addition, we did not observe any effects of transfection and subsequent incorporation into Duragen Plus™ on key regenerative properties of NSCs including viability, stemness, proliferation and differentiation. Transgene expression was maintained in both the NSC population and in the daughter cells, albeit restricted to astrocytes. This suggests that, while further investigation is necessary, a multistep protocol involving magnetofection and stem cell encapsulation into Duragen Plus™ has the potential to be undertaken safely for clinical application.

Taken together, our data strongly support the concept of safely deploying a surgical grade and widely used biomaterial to develop implantable plugs of nanoengineered stem cells for combinatorial therapies in the damaged CNS and may also be applicable to a wide range of other neural transplant types. Indeed, recent work from our laboratory (unpublished data) suggest that the Duragen Plus™ matrix can also support the growth of the major transplant population of oligodendrocyte precursor cells, and their differentiation into oligodendrocytes with applications in demyelinating injuries of the brain and spinal cord. A critical but challenging next step will be robust molecular evaluation of the safety of stem cells engineered for neurotrophin release, and incorporated into a biomaterial matrix, which will require development of methods to isolate cells from the biomatrix. Further, as surgical grade materials in highly aligned conformations are developed for peripheral nerve injuries, we can predict similar advances will ensue with CNS materials that show mimicry of native spinal cord micro-architecture. We recently also showed that pre-labelling of transplant populations with clinical grade nanoparticles can be used to detect transplant cells incorporated into polymer matrices using magnetic resonance imaging [56], offering further advantages for clinical cell therapy. Further testing of such encapsulating matrices using live animal models of neurological injury with assessment of functional neurological recovery, and assessment of the compatibility of the biomaterials to support growth of human transplant populations is needed to advance the use of such an approach for clinical cell therapy applications. The next steps in evaluation of such novel cell- biomaterial constructs (ideally in chronic injuries with behavioural testing), will need to account for a number of confounding influences on transplant cell retention and survival. These include the impact of biomaterial breakdown and remodelling by incorporated transplant cells and host immune responses to the introduced constructs within neurological injury sites, whilst controlling for the potential regeneration enhancing properties of the material alone.

4. Materials and Methods

4.1 Reagents

All culture grade plastics and culture medium reagents were from Thermo Fisher Scientific (Loughborough, UK) or Sigma Aldrich (Dorset, UK) unless otherwise specified. Human recombinant Epidermal Growth Factor (EGF) was from R&D Systems (Minnesota, USA) and human recombinant basic Fibroblast Growth Factor (FGF-2) was from Peprotech (London, UK). Fetal bovine serum was from Biosera (Nuiallé, France). Duragen Plus™ was a kind gift from Integra LifeSciences (New Jersey, USA). Calcein was from VWR (Pennsylvania, USA), Ethidium homodimer-1 and Hoechst were from Thermo Fisher Scientific, UK, and the Click-iT EDU Imaging Kit was from Invitrogen (California, USA). Bovine serum albumin (BSA) and

paraformaldehyde (PFA) were from Thermo Fisher Scientific, normal donkey serum (NDS) was from Stratech Scientific (Suffolk, UK), and Triton X-100 was from Sigma Aldrich. Primary antibodies were anti-nestin from BD Biosciences (Oxford, UK), anti-sox-2 from Millipore (Massachusetts, USA), purified anti-neuron-specific class III beta-tubulin (TUJ1) from Biolegend (California, USA); anti-Glial Fibrillary Acidic Protein (GFAP) from Thermo Fisher Scientific; anti-Myelin Basic Protein (MBP) from BioRad (California, USA) and the TurboGFP antibody from Thermo Fisher Scientific. Secondary antibodies were Fluorescein isothiocyanate (FITC)-conjugated donkey anti-mouse, -rabbit and -rat, cyanine 3 (CY3) donkey anti-mouse, -rabbit and –rat which were all from Stratech Scientific. Vectashield mounting medium with 4', 6-diamidino-2-phenylindole (DAPI) and Vectashield mounting medium for fluorescence were from Vector Laboratories (Peterborough, UK).

pMC.EF1-MCS-IRES-GFP-SV40PolyA, GelRed, MC-Easy™ Growth Medium and MC-Easy™ Induction Medium were from Cambridge Biosciences (Cambridge, UK). MC-Easy™ Minicircle DNA Production kit was from System Biosciences (California, USA). QIAprep miniprep kit and QIA maxiprep kit were from Qiagen (Manchester, UK). LB Agar and LB broth were from Thermo Fisher Scientific. Kanamycin was from Sigma Aldrich. EcoRI was from Promega (Wisconsin, USA). Agarose was from Appleton Woods (Birmingham, UK). NeuroMag transfection reagent was from Oz Biosciences (Marseilles, France) and the Magnefect-nano 24-magnet array system was from NanoTherics (Stoke-on-Trent, UK); see Pickard et al. [57] for nanoparticle and magnetic plate details.

4.2. SEM characterisation of acellular Duragen Plus™

Samples were prepared using the osmium tetroxide (OsO_4) and thiocarbohydrazide multiple step protocol known as OTOTO [58]. Samples were first fixed in 2.5% glutaraldehyde diluted in 0.1M Sodium Cacodylate buffer with 2mM calcium chloride for two h. All washes were carried out in Sodium Cacodylate buffer. After the first wash, samples were incubated with 1% OsO_4 for one hour then washed again. A series of four incubations followed this: (1) thiocarbohydrazide for 20 minutes then (2) OsO_4 for two h, (3) thiocarbohydrazide for 20 minutes, and (4) OsO_4 for two h. Samples were then dehydrated in a series of ethanol solutions of increasing concentration. Critical point drying was carried out using liquid carbon dioxide. Samples were then mounted on aluminium stubs in preparation for SEM. SEM was carried out at the standard setting of 5Kv. Images were taken at x100, x1000 and x10,000 magnification. For quantification of the pore size in Duragen Plus™, five fields were taken at x1000 and included fields from the four corners and the centre of the Duragen Plus™ sample. Using ImageJ (www.imagej.net), the largest diameter from each pore was measured.

4.3 NSC culture

Primary cultures of NSCs were derived from the subventricular zone of postnatal day one to three CD1 mice and propagated as neurospheres in accordance with previously published methods [42]. NSCs were passaged using an Accutase-DNaseI mix once confluent (six to ten days) and NSCs from passages 1-3 were used for experiments. Culture medium comprised of Dulbecco's Modified Eagle Medium: Ham's F12 (3:1), 4 ng/mL Heparin, 2% B27, 20 ng/mL Epidermal Growth Factor, 20 ng/mL basic Fibroblast Growth Factor, 50 U/mL penicillin and 50 U/mL streptomycin at 37°C (referred to from herein as neurosphere medium). Cultures underwent a 50% exchange of medium every two to three days.

4.4 Incorporating NSCs into the Duragen Plus™ matrix

To optimize the visualization of cells within Duragen Plus™, the material required slicing to 250 µm (data for optimization of thickness not shown) using a McIlwain Tissue Chopper under sterile conditions following a protocol adapted from Weightman *et al.* [59]. Neurospheres were dissociated (Accutase-DNaseI mix) and 300 µL seeded onto sliced samples of Duragen Plus™ in 24 well plates at a cell density of $1x10^6$ cells/mL in neurosphere medium. NSC-seeded Duragen Plus™ samples were then incubated at 37°C in 5% CO2/ 95% humidified air until fixation at the experimental time points (described in section 4.11). To investigate the effects of Duragen Plus™ on NSC differentiation, after 48 h in neurosphere medium, this was exchanged for differentiation medium (components as for neurosphere medium minus growth factors with the addition of 1% fetal bovine serum) and samples underwent a 50% differentiation medium exchange every two to three days.

4.5 Genetic engineering of NSCs

mcGFP were produced using the parental plasmid pMC.EF1-MCS-IRES-GFP-SV40PolyA and the MC-EasyTM Minicircle DNA Production kit as per the manufacturer's instructions using the E. coli strain ZYCY10P3S2T. Plasmid DNA was isolated using a QIAprep maxiprep kit as per the manufacturer's instructions with the following amendments: 20 mL of Buffers P1, P2 and P3 were used. Conformation of plasmid size was performed using an EcoRI restriction digest and subsequent electrophoresis with a 1% agarose gel in 1xTAE buffer prestained with 0.0005% GelRed (2 h, 100V).

The method of transfection of neurospheres used here has previously provided efficient transfection [24,60]. NSCs were passaged after reaching confluence using accutase and DNase as previously described, and 500 µL of a single cell suspension at 1 $x10^5$ cells/mL was added to each well of a 24-well Nunc non-treated multidish. NSCs were allowed 24 h

to form neurospheres prior to transfection. NeuroMag, a commercial MNP was used for all transfections. mcGFP and NeuroMag particles were suspended in a solution of 3:1 DMEM: F12 and incubated for 20 minutes to allow the formation of complexes. 50 µl of solution was added to each well for transfection containing 125 ng of mcGFP and 0.435 µl of NeuroMag iron oxide nanoparticles (a ratio used previously [42]), 50 µl of the same DMEM: F12 solution without DNA or nanoparticles was added to each control well. Each plate was then placed on top of a nanoTherics magnefect-nano 24-magnet array system. The programme was set to F=4Hz to produce an oscillating field for 30 minutes. The plate was then removed and placed at 37°C in 5% CO_2/ 95% humidified air. After 16 h, transfection of neurospheres was confirmed using an Axio Observer.Z1 in combination with an AxioCam MRm with Zen two. Following confirmation of transfection, neurospheres were either left to grow for two and four days before protein isolation was performed or transferred onto pre-prepared 250 µm slices of Duragen Plus™. Constructs were then incubated at 37°C in 5% CO_2/ 95% humidified air until their relevant assay time point.

4.6 Isolation of proteins from genetically engineered NSCs and proteomic analysis

Following transfection, NSCs were left to grow as neurospheres for two and four days along with untransfected control counterparts. Cells were washed 1X in PBS before dissociation using TrypLE (RT, <5 mins). Cells were then pelleted by centrifugation before washing 3X in 50 mM Ammonium Bicarbonate (Ambic) with centrifugation in between each wash. After removal of the final wash, lysis buffer (100 µl; 0.1% Rapigest, 1% DNase made up in 50 mM Ambic) was added and probe sonication was performed on ice (3 cycles of 15 seconds on, 5 seconds off, 20% power). Debris was removed by centrifugation and the protein content of the supernatant was determined using a Bradford assay. Protein concentrations were normalised to 100 µg for each sample. Each solution was then incubated with 10 mM DTT whilst shaking (80°C, 15 min) before addition of iodoacetamide (to a final concentration of 20 mM, 30 min, RT and in the dark). Trypsin (2 µg) was then added to each sample and incubated at 37°C for 16 h. Remaining trypsin activity was terminated, and Rapigest precipitated, by addition of trifluoroacetic acid (1%) and acetonitrile (2%) with shaking (60°C, 2 h). Rapigest was pelleted and removed by centrifugation and supernatant taken and stored at -80°C before further analysis.

4.7 LC-MS/MS for Ion Library Creation and SWATH Acquisition

IDA (information dependent acquisition) and SWATH MS were performed using a TripleTOF 6600 mass spectrometer (SCIEX) coupled to a nanoLC 425 (SCIEX) operated in trap-elute configuration. Samples were loaded onto a YMC Triart C18 trap column (5 x 0.5 mm) at a flow rate of 10 µl/min for 4 minutes in 0.1% formic acid, 2% acetonitrile in water, before

being separated on a YMC Triart C18 column (3 µm, 0.3 x 150 mm) at 5 µl/min. For IDA analyses a linear gradient from 2 to 35% mobile phase B over 118 min was used, followed by 35 to 40% B over 5 min; for SWATH analyses a shorter gradient was employed: linear from 2 to 35% B over 38 min, followed by 35 to 40% B over 5 min. Mobile phases: A, 0.1% formic acid in water; B, 0.1% formic acid in acetonitrile. 4 µg sample plus 0.1 µl HRM calibration peptide standard (Biognosys, Zurich, Switzerland) was analysed per injection for SWATH analyses; for IDA analyses approximately 5 µg sample pool plus 0.125 µl HRM calibration peptides was analysed per injection.

4.8 Ion library creation for SWATH Analysis

An ion library for mining the SWATH data was created by combining IDA analysis of a pooled sample with a recent mouse adult αNSC ion library published by Braccia *et al.* [61]. For pooled sample analysis, IDA was combined with gas phase fractionation. The precursor ion *m/z* range of interest was divided into 5 sections, each containing an approximately equal number of precursors: *m/z* 400 – 487, 486 – 574, 573 – 677, 676 – 830 and 829 – 1250. A separate IDA method was created for each gas phase fraction. A TOF MS survey scan (accumulation time 250 ms) was performed over the *m/z* range corresponding to the relevant gas phase fraction, followed by up to 50 dependent MS/MS scans (each with accumulation time 50 ms). MS/MS Spectra were acquired over the range 100 - 1500 *m/z* for precursors with charge state 2 – 5. Collision energies for MS/MS were calculated based on precursor size and charge using the SCIEX recommended rolling collision energy equations (https://sciex.com/community/application-discussions/proteomics/swath/data-acquisition/crowdsourcing-optimized-rolling-collision-energy-curves-for-id-and-swath-acquisition). The pooled sample was analysed twice using each IDA method. The combined data from the IDA analyses were submitted to database searching using ProteinPilot software (SCIEX) against a Uniprot mouse fasta database containing 83588 protein sequences (downloaded 24th May 2018). Protein identifications corresponding to the ProteinPilot 1% false discovery rate group (3490 proteins) were uploaded to the OneOmics data environment hosted on the BaseSpace cloud (http://basespace.illumina.com) via the CloudConnect microapplication for PeakView software (SCIEX). The αNSC library created by Braccia *et al*. [61] was also uploaded to BaseSpace. The two ion libraries were combined at the Extractor stage of OneOmics processing.

4.9 SWATH MS DIA

A variable window SWATH acquisition method was created using the SWATH Variable Window Calculator version 1.1 (SCIEX) based on TOF MS data of the pooled sample. The method contained 75 variable SWATH windows covering the precursor *m/z* range 400 –

1250. For each experimental cycle, a TOF MS scan with accumulation time 50 ms was performed over the *m/z* range 400 – 1250, followed by 75 SWATH MS/MS scans each with accumulation time 25 ms, *m/z* range 100 – 1500. Total cycle time was 1.98 sec. Collision energies for MS/MS were calculated as for IDA experiments, with a collision energy spread of 5V. Sample analysis order was randomised; each sample was analysed three times.

4.10 SWATH MS Data analysis in OneOmics

SWATH MS data was uploaded to BaseSpace using the CloudConnect microapplication for PeakView. 134,062 peptide transitions from 22,344 peptides were observed as having matches within the ion library used [61] *et al*, attributable to 4,107 proteins. Data were submitted to PeptideAtlas under identifier PASS01434. Using the Analytics module of OneOmics Cloud Browser (SCIEX, Framingham, MA), 213 proteins were reliably observed at a 65% confidence and 0.15 reproducibility across both conditions, both timepoints and all three litters.

4.11 Characterisation of NSCs in Duragen Plus™

24 h, 8 days and 12 days after seeding NSCs in Duragen Plus™, cell viability, proliferation and immunocytochemistry assays were performed. For transfected cells seeded into Duragen Plus™, day 0 refers to the day of transfection and day 1 is when cells were added to the constructs. For differentiation, neurosphere medium was changed to differentiation medium at two days post transfection and one day post seeding into Duragen Plus™. Here, transfected NSC behaviour was assayed at day 2 and differentiated cells assayed at day 9.

To assess viability a live-dead assay was conducted which comprised 4 µM calcein, 6 µM ethidium homodimer-1, and 2 µg/mL Hoechst nuclear stain in phosphate buffered saline (PBS) incubated with samples for one hour. Proliferation assays were performed using a Click-iT EdU imaging kit according to the manufacturer's instructions except where incubation times and washes were increased as follows: Component A was incubated for 16 h with NSCs or differentiated cells in Duragen Plus™. Constructs were then fixed with 4% PFA for 30 minutes. Samples were washed four times with 3% bovine serum albumin (BSA) in PBS then 0.5% Triton X-100 was added to each well for 40 minutes. Once again, the construct was washed four times with BSA. The EdU detection cocktail was prepared in accordance with the Invitrogen guidelines and incubated with the sample for one hour, protected from light. Constructs were washed in BSA twice and then PBS twice before the ICC protocol was carried out to identify nuclei and either nestin positive cells at 24 h or GFAP positive cells at eight days.

For identification of specific neural cell types and morphologies, immunocytochemistry was performed. Here, samples were incubated with 4% paraformaldehyde (PFA) for 20 minutes and then washed with PBS three times. Each sample was blocked for 30 minutes with a solution of 5% NDS in PBS-0.3% Triton X-100. Primary antibody diluted in blocker solution was added and incubated overnight. Following this, the primary antibody was removed, and the construct was washed with PBS three times for five minutes each. Again, the sample was blocked for a further 30 minutes with the blocker. Then an appropriate secondary antibody diluted in blocker (1:200) was added for up to three h, to allow penetration of Duragen Plus™. Each sample was incubated with 2 µg/mL Hoechst for one hour before finally washing 3 times with PBS. Primary antibody dilutions were nestin (1:200) and Sox-2 (1:1000) to detect NSCs, GFAP (1:500) for astrocytes, TUJ1 (1:1000) for neurons and MBP (1:200) for oligodendrocytes.

4.12 Fluorescence microscopy of NSCs in Duragen Plus™

All fluorescence imaging was carried out using an Axio Observer.Z1 in combination with an AxioCam MRm (black and white camera) with Zen two (blue edition) software. For all assays five fields were randomly selected at x200 magnification. A stack of images was taken as the focus moved upwards to produce a Z-stack; this was carried out at each field with the interval fixed at 5 µm between each image. The top and bottom of the stack was allocated when the last visible cell went out of focus.

4.13 Quantification and statistical analysis of histological data

Quantification was carried out utilising ImageJ free software on stacks of images taken for live-dead assays, EdU assays, NSC markers and differentiation markers at the allotted time points. For quantification of axon length at day eight, 12 and 16, each Tuj 1 field was surveyed for axons extending within the same plane. Often due to the 3D nature of the construct axons would transverse the layers of the stack making measurements difficult. Axons were only selected for measurement if the cell body and full length of the axon could be visualised in one plane. Of the axons that met the stated criteria, the freehand line tool in ImageJ was utilised to mark from the cell body to the furthest point of the axon, following its curvature. This distance was measured.

The cellular distribution was quantified in the vertical plane at 48 h and eight days. There were five fields per Duragen Plus™ sample as described above. The average number of cells per corner field or central field were calculated to determine if there was a preferential distribution in one of the sections. Analysis of the vertical distribution was also carried out by imaging cell nuclei. Z-stacks were imaged at 5µm intervals. The top and bottom of the matrix

was defined as the point where the first/ last fibre was in focus using phase microscopy. Nuclei per image were counted and converted to a percentage of the total number of images in that z-stack. The average number of cells at each one percent interval was calculated.

Data is represented as mean ± the standard error of the mean with 'n' referring to the number of different cultures (derived from a different litter) within each experiment. Two sample T tests were used to compare between two groups. Grouped data was interrogated by a one-way analysis of variance (ANOVA) and Bonferroni's multiple comparison test was used to determine statistical differences between groups. All statistical tests were performed using MiniTab software.

References

[1] Brosius Lutz, A.; Barres, B.A.; Lutz, A.B.; Barres, B.A.; Brosius Lutz, A.; Barres, B.A.

Contrasting the Glial Response to Axon Injury in the Central and Peripheral Nervous Systems. *Dev. Cell*, **2014**, *28*, 7–17.

[2] Burda, J.E.E.; Sofroniew, M.V. V. Reactive Gliosis and the Multicellular Response to CNS Damage and Disease. *Neuron*, **2014**, *81*, 229–248.

[3] Falk, A.; Holmström, N.; Carlén, M.; Cassidy, R.; Lundberg, C.; Frisén, J. Gene Delivery to Adult Neural Stem Cells. *Exp. Cell Res.*, **2002**, *279*, 34–39.

[4] Mac, G.T.; Wu, P.; Ye, Y.; Svendsen, C.N. Transduction of Human Neural Progenitor Cells Using Recombinant Adeno-Associated Viral Vectors. *Cell*, **2002**, *9*, 245–255.

[5] Kameda, M.; Shingo, T.; Takahashi, K.; Muraoka, K.; Kurozumi, K.; Yasuhara, T.; Maruo, T.; Tsuboi, T.; Uozumi, T.; Matsui, T.; Miyoshi, Y.; Hamada, H.; Date, I. Adult Neural Stem and Progenitor Cells Modified to Secrete GDNF Can Protect, Migrate and Integrate after Intracerebral Transplantation in Rats with Transient Forebrain Ischemia. *Eur. J. Neurosci.*, **2007**, *26*, 1462–1478.

[6] Dieterlen, M.-T.; Wegner, F.; Schwarz, S.C.; Milosevic, J.; Schneider, B.; Busch, M.; Römuss, U.; Brandt, A.; Storch, A.; Schwarz, J. Non-Viral Gene Transfer by Nucleofection Allows Stable Gene Expression in Human Neural Progenitor Cells. *J. Neurosci. Methods*, **2009**, *178*, 15–23.

[7] Elsabahy, M.; Nazarali, A.; Foldvari, M. Non-Viral Nucleic Acid Delivery: Key Challenges and Future Directions. *Curr. Drug Deliv.*, **2011**, *8*, 235–244.

[8] Mintzer, M.A.; Simanek, E.E. Nonviral Vectors for Gene Delivery. *Chem. Rev.*, **2009**, *109*, 259–302.

[9] Trounson, A.; Mcdonald, C. Stem Cell Therapies in Clinical Trials: Progress and Challenges. *Cell Stem Cell*, **2015**, *17*, 11–22.

[10] Mooney, D.J.; Vandenburgh, H. Cell Delivery Mechanisms for Tissue Repair. *Cell Stem Cell*, **2008**, *2*, 205–213.

[11] Mothe, A.J.; Tam, R.Y.; Zahir, T.; Tator, C.H.; Shoichet, M.S. Repair of the Injured Spinal Cord by Transplantation of Neural Stem Cells in a Hyaluronan-Based Hydrogel. *Biomaterials*, **2013**, *34*, 3775–3783.

[12] Lepore, A.C.; Han, S.S.W.; Tyler-Polsz, C.J.; Cai, J.; Rao, M.S.; Fischer, I. Differential Fate of Multipotent and Lineage-Restricted Neural Precursors Following Transplantation into the Adult CNS. *Neuron Glia Biol.*, **2004**, *1*, 113–126.

[13] Teng, Y.D.; Lavik, E.B.; Qu, X.; Park, K.I.; Ourednik, J.; Zurakowski, D.; Langer, R.; Snyder, E.Y. Functional Recovery Following Traumatic Spinal Cord Injury Mediated by a Unique Polymer Scaffold Seeded with Neural Stem Cells. *Proc. Natl. Acad. Sci. U. S. A.*, **2002**, *99*, 3024–3029.

[14] Lu, P.; Wang, Y.; Graham, L.; McHale, K.; Gao, M.; Wu, D.; Brock, J.; Blesch, A.; Rosenzweig, E.S.; Havton, L.A.; Zheng, B.; Conner, J.M.; Marsala, M.; Tuszynski, M.H. Long-Distance Growth and Connectivity of Neural Stem Cells after Severe Spinal Cord Injury. *Cell*, **2012**, *150*, 1264–1273.

[15] Wang, J.-M.; Zeng, Y.-S.; Wu, J.-L.; Li, Y.; Teng, Y.D. Cograft of Neural Stem Cells and Schwann Cells Overexpressing TrkC and Neurotrophin-3 Respectively after Rat Spinal Cord Transection. *Biomaterials*, **2011**, *32*, 7454–7468.

[16] Li, X.; Xiao, Z.; Han, J.; Chen, L.; Xiao, H.; Ma, F.; Hou, X.; Li, X.; Sun, J.; Ding, W.; Zhao, Y.; Chen, B.; Dai, J. Promotion of Neuronal Differentiation of Neural Progenitor Cells by Using EGFR Antibody Functionalized Collagen Scaffolds for Spinal Cord Injury Repair. *Biomaterials*, **2013**, *34*, 5107–5116.

[17] Liu, C.; Huang, Y.; Pang, M.; Yang, Y.; Li, S.; Liu, L.; Shu, T.; Zhou, W.; Wang, X.; Rong, L.; Liu, B. Tissue-Engineered Regeneration of Completely Transected Spinal Cord Using Induced Neural Stem Cells and Gelatin-Electrospun Poly (Lactide-Co-Glycolide)/Polyethylene Glycol Scaffolds. *PLoS One*, **2015**, *10*, e0117709.

[18] Van Norman, G.A. Drugs, Devices, and the FDA: Part 1: An Overview of Approval Processes for Drugs. *JACC Basic to Transl. Sci.*, **2016**, *1*, 170–179.

[19] Sade, B.; Oya, S.; Lee, J.H. Non-Watertight Dural Reconstruction in Meningioma Surgery: Results in 439 Consecutive Patients and a Review of the Literature. *J. Neurosurg.*, **2011**, *114*, 714–718.

[20] Pena, C. (FDA). *Department of Health and Human Services*; **2015**.

[21] Rabinowitz, L.; Monnerie, H.; Shashidhara, S.; Le Roux, P.D. Growth of Rat Cortical Neurons on DuraGen, a Collagen-Based Dural Graft Matrix. *Neurol. Res.*, **2005**, *27*, 887–894.

[22] Kroemer, G.; Galluzzi, L.; Vandenabeele, P.; Abrams, J.; Alnemri, E.S.; Baehrecke, E.H.; Blagosklonny, M. V; El-Deiry, W.S.; Golstein, P.; Green, D.R.; Hengartner, M.; Knight, R.A.; Kumar, S.; Lipton, S.A.; Malorni, W.; Nuñez, G.; Peter, M.E.; Tschopp, J.; Yuan, J.; Piacentini, M.; Zhivotovsky, B.; Melino, G.; Nomenclature Committee on

Cell Death 2009. Classification of Cell Death: Recommendations of the Nomenclature Committee on Cell Death 2009. *Cell Death Differ.*, **2009**, *16*, 3–11.

[23] Adams, C.F.; Pickard, M.R.; Chari, D.M. Magnetic Nanoparticle Mediated Transfection of Neural Stem Cell Suspension Cultures Is Enhanced by Applied Oscillating Magnetic Fields. *Nanomedicine Nanotechnology, Biol. Med.*, **2013**, *9*, 737–741.

[24] Fernandes, A.R.; Chari, D.M. Part I: Minicircle Vector Technology Limits DNA Size Restrictions on Ex Vivo Gene Delivery Using Nanoparticle Vectors: Overcoming a Translational Barrier in Neural Stem Cell Therapy. *J. Control. Release*, **2016**, *238*.

[25] Bento, A.R.; Quelhas, P.; Oliveira, M.J.; Pêgo, A.P.; Amaral, I.F. Three-Dimensional Culture of Single Embryonic Stem-Derived Neural/Stem Progenitor Cells in Fibrin Hydrogels: Neuronal Network Formation and Matrix Remodelling. *J. Tissue Eng. Regen. Med.*, **2017**, *11*, 3494–3507.

[26] Lin, C.; Liu, C.; Zhang, L.; Huang, Z.; Zhao, P.; Chen, R.; Pang, M.; Chen, Z.; He, L.; Luo, C.; Rong, L.; Liu, B. Interaction of IPSC-Derived Neural Stem Cells on Poly(L-Lactic Acid) Nanofibrous Scaffolds for Possible Use in Neural Tissue Engineering. *Int. J. Mol. Med.*, **2017**.

[27] Kadoya, K.; Lu, P.; Nguyen, K.; Lee-Kubli, C.; Kumamaru, H.; Yao, L.; Knackert, J.; Poplawski, G.; Dulin, J.N.; Strobl, H.; Takashima, Y.; Biane, J.; Conner, J.; Zhang, S.-C.; Tuszynski, M.H. Spinal Cord Reconstitution with Homologous Neural Grafts Enables Robust Corticospinal Regeneration. *Nat. Med.*, **2016**, *22*, 479–487.

[28] Du, B.-L.; Xiong, Y.; Zeng, C.-G.; He, L.-M.; Zhang, W.; Quan, D.-P.; Wu, J.-L.; Li, Y.; Zeng, Y.-S. Transplantation of Artificial Neural Construct Partly Improved Spinal Tissue Repair and Functional Recovery in Rats with Spinal Cord Transection. *Brain Res.*, **2011**, *1400*, 87–98.

[29] Integra LifeSciences Corporation. Ultra Pure Collagen ™ Dural Repair, **2009**.

[30] Zhuo, F.; Liu, X.; Gao, Q.; Wang, Y.; Hu, K.; Cai, Q. Injectable Hyaluronan-Methylcellulose Composite Hydrogel Crosslinked by Polyethylene Glycol for Central Nervous System Tissue Engineering. *Mater. Sci. Eng. C*, **2017**, *81*, 1–7.

[31] Stewart, A.N.; Matyas, J.J.; Welchko, R.M.; Goldsmith, A.D.; Zeiler, S.E.; Hochgeschwender, U.; Lu, M.; Nan, Z.; Rossignol, J.; Dunbar, G.L. SDF-1 Overexpression by Mesenchymal Stem Cells Enhances GAP-43-Positive Axonal

Growth Following Spinal Cord Injury. *Restor. Neurol. Neurosci.*, **2017**, *35*, 395–411.

[32] Stewart, A.N.; Kendziorski, G.; Deak, Z.M.; Brown, D.J.; Fini, M.N.; Copely, K.L.; Rossignol, J.; Dunbar, G.L. Co-Transplantation of Mesenchymal and Neural Stem Cells and Overexpressing Stromal-Derived Factor-1 for Treating Spinal Cord Injury. *Brain Res.*, **2017**, *1672*, 91–105.

[33] Shakhbazau, A.; Shcharbin, D.; Bryszewska, M.; Kumar, R.; Wobma, H.M.; Kallos, M.S.; Goncharova, N.; Seviaryn, I.; Kosmacheva, S.; Potapnev, M.; Midha, R. Non-Viral Engineering of Skin Precursor-Derived Schwann Cells for Enhanced NT-3 Production in Adherent and Microcarrier Culture. *Curr. Med. Chem.*, **2012**, *19*, 5572–5579.

[34] Lavdas, A.A.; Chen, J.; Papastefanaki, F.; Chen, S.; Schachner, M.; Matsas, R.; Thomaidou, D. Schwann Cells Engineered to Express the Cell Adhesion Molecule L1 Accelerate Myelination and Motor Recovery after Spinal Cord Injury. *Exp. Neurol.*, **2010**, *221*, 206–216.

[35] Cai, P.; Sun, G.; Cai, P.; Oudega, M.; Xiao, R.; Wang, X.; Li, W.; Shu, Y.; Cai, C.; Yang, H.; Shan, X.; Luo, W. Survival of Transplanted Neurotrophin-3 Expressing Human Neural Stem Cells and Motor Function in a Rat Model of Spinal Cord Injury. *Neural Regen. Res.*, **2009**, *4*, 485–491.

[36] Bohl, D.; Liu, S.; Blanchard, S.; Hocquemiller, M.; Haase, G.; Heard, J.-M. Directed Evolution of Motor Neurons from Genetically Engineered Neural Precursors. *Stem Cells*, **2008**, *26*, 2564–2575.

[37] Ruitenberg, M.J.; Levison, D.B.; Lee, S. V.; Verhaagen, J.; Harvey, A.R.; Plant, G.W. NT-3 Expression from Engineered Olfactory Ensheathing Glia Promotes Spinal Sparing and Regeneration. *Brain*, **2005**, *128*, 839–853.

[38] Ruitenberg, M.J.; Plant, G.W.; Hamers, F.P.T.; Wortel, J.; Blits, B.; Dijkhuizen, P.A.; Gispen, W.H.; Boer, G.J.; Verhaagen, J. Ex Vivo Adenoviral Vector-Mediated Neurotrophin Gene Transfer to Olfactory Ensheathing Glia: Effects on Rubrospinal Tract Regeneration, Lesion Size, and Functional Recovery after Implantation in the Injured Rat Spinal Cord. *J. Neurosci.*, **2003**, *23*, 7045–7058.

[39] Taha, M.F. Cell Based-Gene Delivery Approaches for the Treatment of Spinal Cord Injury and Neurodegenerative Disorders. *Curr. Stem Cell Res. Ther.*, **2010**, *5*, 23–36.

[40] Carwardine, D.; Wong, L.-F.; Fawcett, J.W.; Muir, E.M.; Granger, N. Canine Olfactory

Ensheathing Cells from the Olfactory Mucosa Can Be Engineered to Produce Active Chondroitinase ABC. *J. Neurol. Sci.*, **2016**, *367*, 311–318.

[41] Pickard, M.; Adams, C.; Barraud, P.; Chari, D. Using Magnetic Nanoparticles for Gene Transfer to Neural Stem Cells: Stem Cell Propagation Method Influences Outcomes. *J. Funct. Biomater.*, **2015**, *6*, 259–276.

[42] Pickard, M.R.; Barraud, P.; Chari, D.M. The Transfection of Multipotent Neural Precursor/Stem Cell Transplant Populations with Magnetic Nanoparticles. *Biomaterials*, **2011**, *32*, 2274–2284.

[43] Mothe, A.J.; Kulbatski, I.; Parr, A.; Mohareb, M.; Tator, C.H. Adult Spinal Cord Stem/Progenitor Cells Transplanted as Neurospheres Preferentially Differentiate into Oligodendrocytes in the Adult Rat Spinal Cord. *Cell Transplant.*, **2008**, *17*, 735–751.

[44] Karbanová, J.; Mokrý, J.; Kotingová, L. Neural Stem Cells Transplanted into Intact Brains as Neurospheres Form Solid Grafts Composed of Neurons, Astrocytes and Oligodendrocyte Precursors. *Biomed. Pap. Med. Fac. Univ. Palacky. Olomouc. Czech. Repub.*, **2004**, *148*, 217–220.

[45] Vogel, C.; Marcotte, E.M. Insights into the Regulation of Protein Abundance from Proteomic and Transcriptomic Analyses. *Nat. Rev. Genet.*, **2012**, *13*, 227–232.

[46] Liu, Y.; Beyer, A.; Aebersold, R. On the Dependency of Cellular Protein Levels on MRNA Abundance. *Cell*, **2016**, *165*, 535–550.

[47] Lin, D.; Alborn, W.E.; Slebos, R.J.C.; Liebler, D.C. Comparison of Protein Immunoprecipitation-Multiple Reaction Monitoring with ELISA for Assay of Biomarker Candidates in Plasma. *J. Proteome Res.*, **2013**, *12*, 5996–6003.

[48] Sedic, M.; Gethings, L.A.; Vissers, J.P.C.; Shockcor, J.P.; McDonald, S.; Vasieva, O.; Lemac, M.; Langridge, J.I.; Batinić, D.; Pavelić, S.K. Label-Free Mass Spectrometric Profiling of Urinary Proteins and Metabolites from Paediatric Idiopathic Nephrotic Syndrome. *Biochem. Biophys. Res. Commun.*, **2014**, *452*, 21–26.

[49] Delaney, A.M.; Adams, C.F.; Fernandes, A.R.; Al-Shakli, A.F.; Sen, J.; Carwardine, D.R.; Granger, N.; Chari, D.M. A Fusion of Minicircle DNA and Nanoparticle Delivery Technologies Facilitates Therapeutic Genetic Engineering of Autologous Canine Olfactory Mucosal Cells. *Nanoscale*, **2017**, *9*, 8560–8566.

[50] Miller, S.; Coveney, C.; Johnson, J.; Farmaki, A.-E.; Gupta, N.; Tobin, M.D.; Wain, L.

V.; McCormack, F.X.; Boocock, D.J.; Johnson, S.R. The Vitamin D Binding Protein Axis Modifies Disease Severity in Lymphangioleiomyomatosis. *Eur. Respir. J.*, **2018**, *52*, 1800951.

[51] Conti, L.; Cattaneo, E. Neural Stem Cell Systems: Physiological Players or in Vitro Entities? *Nat. Rev. Neurosci.*, **2010**, *11*, 176–187.

[52] Gliga, A.R.; Edoff, K.; Caputo, F.; Källman, T.; Blom, H.; Karlsson, H.L.; Ghibelli, L.; Traversa, E.; Ceccatelli, S.; Fadeel, B. Cerium Oxide Nanoparticles Inhibit Differentiation of Neural Stem Cells. *Sci. Rep.*, **2017**, *7*, 1–20.

[53] Gotoh, H.; Nomura, T.; Ono, K. Glycogen Serves as an Energy Source That Maintains Astrocyte Cell Proliferation in the Neonatal Telencephalon. *J. Cereb. Blood Flow Metab.*, **2017**, *37*, 2294–2307.

[54] Corbet, C. Stem Cell Metabolism in Cancer and Healthy Tissues: Pyruvate in the Limelight. *Frontiers in Pharmacology*, **2018**, *8*.

[55] Kamada, F.; Aoki, Y.; Narisawa, A.; Abe, Y.; Komatsuzaki, S.; Kikuchi, A.; Kanno, J.; Niihori, T.; Ono, M.; Ishii, N.; Owada, Y.; Fujimura, M.; Mashimo, Y.; Suzuki, Y.; Hata, A.; Tsuchiya, S.; Tominaga, T.; Matsubara, Y.; Kure, S. A Genome-Wide Association Study Identifies RNF213 as the First Moyamoya Disease Gene. *J. Hum. Genet.*, **2011**, *56*, 34–40.

[56] Adams, C.F.; Delaney, A.M.; Carwardine, D.R.; Tickle, J.; Granger, N.; Chari, D.M. Nanoparticle-Based Imaging of Clinical Transplant Populations Encapsulated in Protective Polymer Matrices. *Macromol. Biosci.*, **2018**, *1800389*, 1800389.

[57] Pickard, M.; Chari, D. Enhancement of Magnetic Nanoparticle-Mediated Gene Transfer to Astrocytes by 'Magnetofection': Effects of Static and Oscillating Fields. *Nanomedicine*, **2010**, *5*, 217–232.

[58] Fernandes, A.R.; Adams, C.F.; Furness, D.N.; Chari, D.M. Early Membrane Responses to Magnetic Particles Are Predictors of Particle Uptake in Neural Stem Cells. *Part. Part. Syst. Charact.*, **2015**, *32*, 661–667.

[59] Weightman, A.P.; Pickard, M.R.; Yang, Y.; Chari, D.M. An in Vitro Spinal Cord Injury Model to Screen Neuroregenerative Materials. *Biomaterials*, **2014**, *35*, 3756–3765.

[60] Fernandes, A.R.; Chari, D.M. Part II: Functional Delivery of a Neurotherapeutic Gene to Neural Stem Cells Using Minicircle DNA and Nanoparticles: Translational

Advantages for Regenerative Neurology. *J. Control. Release*, **2016**, *238*.

[61] Braccia, C.; Espinal, M.P.; Pini, M.; De Pietri Tonelli, D.; Armirotti, A. A New SWATH Ion Library for Mouse Adult Hippocampal Neural Stem Cells. *Data Br.*, **2018**, *18*, 1–8.

Supplementary Information

Safe nanoengineering and encapsulation of neural stem cells into a neurosurgical grade biomaterial, DuraGen™ for protected cell delivery applications

Louise Finch[1], Sarah Harris[1], Georgios Solomou[1], Jon Sen[1,2], Nikolaos Tzerakis[3], Richard Emes[4,5], Catherine S Lane[6], Sarah Hart[1], Christopher Adams[7] and Divya Maitreyi Chari [1,*]

[1]School of Medicine, Keele University, Stoke-on-Trent, ST5 5BG; d.chari@keele.ac.uk

[2]Neurosurgery department, HCA Healthcare, London, W1G 8BJ; j.sen@keele.ac.uk

[3]Neurosurgery department, University Hospitals of North Midlands, Stoke-on-Trent, ST4 6QG; Nikolaos.Tzerakis@uhnm.nhs.uk.

[4]Advanced Data Analysis Centre, University of Nottingham, Sutton Bonnington, Leicestershire, LE12 5RD, UK.

[5]School of Veterinary Medicine and Science, University of Nottingham, Sutton Bonnington, Leicestershire, LE12 5RD, UK; Richard.Emes@nottingham.ac.uk.

[6]Sciex, Phoenix House, Lakeside Drive, Centre Park, Warrington WA1 1RX; Cathy.Lane@sciex.com.

[7]Faculty of Natural Sciences, Keele University, Stoke-on-Trent, ST5 5BG; c.adams@keele.ac.uk.

*Correspondence: d.chari@keele.ac.uk

Supplementary results: *Tables showing significantly dysregulated proteins between the indicated two experimental groups.*

Protein ID	*Fold change*	*P-value*
tr|A0A171EBL2|A0A171EBL2_MOUSE	6.28	3.98E-03
sp|Q9D023|MPC2_MOUSE	-2.46	5.40E-05

Supplementary Table 1: Transfected day 2 versus control day 2.

Protein ID	*Fold change*	*P-value*
sp|Q8CI94|PYGB_MOUSE	-2.02	2.05E-03
sp|P03995|GFAP_MOUSE	-2.40	3.05E-05

Supplementary Table 2: Transfected day 4 versus control day 4.

Protein ID	*Fold change*	*P-value*
sp|P03995|GFAP_MOUSE	15.61	3.04E-06
tr|Q58EU7|Q58EU7_MOUSE	5.97	1.24E-03
tr|Q3UYM8|Q3UYM8_MOUSE	10.25	1.50E-03
sp|Q8JZU2|TXTP_MOUSE	8.84	1.79E-04
tr|Q3TVI6|Q3TVI6_MOUSE	6.91	1.65E-04
tr|Q3USR5|Q3USR5_MOUSE	5.71	4.53E-05
tr|Q3UJK6|Q3UJK6_MOUSE	5.65	2.26E-03
sp|Q9DBL1|ACDSB_MOUSE	5.61	7.32E-03
sp|Q9CQE8|CN166_MOUSE	5.50	8.34E-04
sp|Q8CI94|PYGB_MOUSE	5.50	2.86E-06
sp|Q80YN3|BCAS1_MOUSE	5.09	3.78E-03
tr|Q6S393|Q6S393_MOUSE	4.68	1.82E-04
tr|Q8C7W8|Q8C7W8_MOUSE	4.55	5.58E-03
tr|Q3TYV5|Q3TYV5_MOUSE	4.54	1.98E-03
tr|Q3UYH9|Q3UYH9_MOUSE	4.15	1.35E-03
tr|Q3UFX6|Q3UFX6_MOUSE	4.08	8.23E-03
tr|Q4FJX4|Q4FJX4_MOUSE	3.90	3.31E-04
sp|O88587|COMT_MOUSE	3.60	4.01E-03
sp|P12382|PFKAL_MOUSE	3.31	4.86E-04
sp|Q9D023|MPC2_MOUSE	3.71	9.57E-03
sp|P70271|PDLI4_MOUSE	3.62	7.47E-05
tr|Q3V1S0|Q3V1S0_MOUSE	3.61	1.63E-05
sp|Q9QYG0|NDRG2_MOUSE	3.44	6.73E-03
sp|P14873|MAP1B_MOUSE	3.38	3.41E-06
sp|P16330|CN37_MOUSE	3.24	1.63E-03
tr|Q3V1C8|Q3V1C8_MOUSE	2.20	4.46E-03
sp|Q9EQ20|MMSA_MOUSE	3.13	1.83E-04
sp|Q61738|ITA7_MOUSE	2.70	1.28E-06
sp|P17751|TPIS_MOUSE	2.67	6.40E-04
tr|Q4VA29|Q4VA29_MOUSE	2.27	6.43E-03
tr|Q80UE5|Q80UE5_MOUSE	2.70	2.46E-03
tr|Q8BRQ9|Q8BRQ9_MOUSE	2.56	1.72E-04
tr|Q3UXR4|Q3UXR4_MOUSE	2.48	1.32E-08
sp|Q9ESW8|PGPI_MOUSE	2.35	5.33E-03
sp|Q9Z0R9|FADS2_MOUSE	2.33	1.82E-04
sp|P26443|DHE3_MOUSE	2.33	1.94E-05
tr|Q6GT24|Q6GT24_MOUSE	2.32	4.90E-03
sp|Q99L13|3HIDH_MOUSE	2.10	1.91E-03
sp|P26040|EZRI_MOUSE	2.27	1.44E-06
sp|Q9R0H0|ACOX1_MOUSE	2.07	2.97E-03
sp|Q01320|TOP2A_MOUSE	-5.87	6.67E-05
sp|Q8VDF2|UHRF1_MOUSE	-3.81	1.93E-04
tr|Q52L97|Q52L97_MOUSE	-2.64	2.53E-03
sp|P49717|MCM4_MOUSE	-3.75	5.78E-03
tr|Q3ULD6|Q3ULD6_MOUSE	-2.94	8.88E-06
tr|Q52KC3|Q52KC3_MOUSE	-2.53	5.41E-04
tr|Q542I2|Q542I2_MOUSE	-2.40	2.38E-03

sp|Q61881|MCM7_MOUSE	-2.68	2.08E-04
tr|Q91ZH2|Q91ZH2_MOUSE	-2.33	5.16E-07
tr|Q8BQ03|Q8BQ03_MOUSE	-2.43	6.96E-07
sp|P97311|MCM6_MOUSE	-2.35	5.74E-03
tr|A2AGS6|A2AGS6_MOUSE	-2.13	2.05E-07
sp|Q8CG48|SMC2_MOUSE	-2.04	2.28E-03
tr|Q99JW7|Q99JW7_MOUSE	-3.34	7.02E-07
tr|Q3U3F6|Q3U3F6_MOUSE	-2.07	3.54E-04
sp|P13864|DNMT1_MOUSE	-2.40	1.85E-04
sp|E9Q5C9|NOLC1_MOUSE	-2.13	1.23E-05
sp|Q8VD75|HIP1_MOUSE	-2.15	4.51E-05
tr|Q497K3|Q497K3_MOUSE	-4.55	1.05E-04

Supplementary Table 3: Control day 4 versus control day 2.

Protein ID	*Fold change*	*P-value*
sp|P03995|GFAP_MOUSE	8.84	7.66E-05
sp|Q8CI94|PYGB_MOUSE	2.91	5.06E-04
sp|Q9D023|MPC2_MOUSE	4.32	5.09E-06
tr|Q3UFX6|Q3UFX6_MOUSE	3.52	3.12E-03
tr|Q3USR5|Q3USR5_MOUSE	2.65	3.63E-03
sp|O89023|TPP1_MOUSE	2.51	4.07E-06
sp|Q9QYG0|NDRG2_MOUSE	2.41	6.88E-03
tr|Q3UYH9|Q3UYH9_MOUSE	2.27	5.60E-03
tr|Q6S393|Q6S393_MOUSE	2.19	7.73E-03
tr|Q544Z7|Q544Z7_MOUSE	2.93	3.26E-03
sp|Q9Z0R9|FADS2_MOUSE	2.68	4.06E-03
tr|Q8BRQ9|Q8BRQ9_MOUSE	2.40	9.01E-03
sp|O09005|DEGS1_MOUSE	2.04	1.68E-04
tr|A0A1Y7VN70|A0A1Y7VN70_MOUSE	2.35	5.03E-04
sp|P12382|PFKAL_MOUSE	2.39	1.46E-10
tr|Q497K3|Q497K3_MOUSE	-3.57	7.76E-04
sp|P33609|DPOLA_MOUSE	-2.33	2.05E-03
sp|P49717|MCM4_MOUSE	-2.28	1.01E-03
sp|Q8VDF2|UHRF1_MOUSE	-2.58	1.52E-05
sp|Q01320|TOP2A_MOUSE	-2.38	9.08E-09

Supplementary Table 4: Transfected day 4 versus transfected day 2.